

Article

Non-Dimensional Analysis of Diffusion Characteristics in Polymer Electrolyte Membrane Fuel Cells with Mismatched Anodic and Cathodic Flow Channels

Hyeok Kim , Geonhwi Kim, Jaeyeon Kim , Dasol Kim, Obeen Kwon, Hongnyoung Yoo, Hyeonjin Cha, Heesoo Choi  and Taehyun Park * 

Department of Mechanical Engineering, Soongsil University, 369 Sangdo-ro, Dongjak-gu, Seoul 06978, Korea; rlagpdhr96@gmail.com (H.K.); machunna@naver.com (G.K.); jaeyeonkim@soongsil.ac.kr (J.K.); rlaek3924@naver.com (D.K.); freedomin1995@soongsil.ac.kr (O.K.); aust26@soongsil.ac.kr (H.Y.); mathyan@soongsil.ac.kr (H.C.); choihs95@soongsil.ac.kr (H.C.)

* Correspondence: taehyunpark@ssu.ac.kr

Abstract: Polymer electrolyte membrane fuel cells were analyzed to investigate changes in the structure of the flow field and operating conditions. The cell performance, which was controlled by adjusting the width of the cathodic channel, improved as the backpressure increases. With the anodic and cathodic flow channels mismatched, the maximum power densities at 3.0 bar for a narrow cathodic channel were 1115 and 1024 mW/cm², and those for a wide cathodic channel were 959 and 868 mW/cm², respectively. The diffusion characteristics were investigated using the non-dimensional numbers *Re* (Reynolds), *Sc* (Schmidt), and *Sh* (Sherwood) to confirm the improvement of mass transport. The narrower the channel or the higher the operating pressure, the larger *Re* was and the smaller *Sc* and *Sh* became. In particular, the wider the anodic channel, the larger the value of *Sh*.

Keywords: polymer electrolyte membrane fuel cell; electrochemical impedance spectroscopy; Sherwood number; Schmidt number; diffusion



Citation: Kim, H.; Kim, G.; Kim, J.; Kim, D.; Kwon, O.; Yoo, H.; Cha, H.; Choi, H.; Park, T. Non-Dimensional Analysis of Diffusion Characteristics in Polymer Electrolyte Membrane Fuel Cells with Mismatched Anodic and Cathodic Flow Channels. *Energies* **2021**, *14*, 8596. <https://doi.org/10.3390/en14248596>

Academic Editor: Calin Iclodean

Received: 17 November 2021

Accepted: 16 December 2021

Published: 20 December 2021

Publisher's Note: MDPI stays neutral with regard to jurisdictional claims in published maps and institutional affiliations.



Copyright: © 2021 by the authors. Licensee MDPI, Basel, Switzerland. This article is an open access article distributed under the terms and conditions of the Creative Commons Attribution (CC BY) license (<https://creativecommons.org/licenses/by/4.0/>).

1. Introduction

Fuel cells are attracting attention as energy conversion devices owing to their high energy efficiency, near-zero emission, and low noise [1,2]. Among them, polymer electrolyte membrane fuel cells (PEMFCs) are recognized as the most promising candidates for various applications such as vehicles, distributed power systems, aerospace applications, and submarines [3–5]. The performance of fuel cells is affected by various conditions (operating temperature, pressure, humidification, etc.), and optimization of these conditions is a practical approach to improve their performance. In addition, the use of a flow field with a suitable design is known to improve the performance [6–8].

Many researchers focusing on improving the operating conditions of PEMFCs have studied the effect of varying the operating pressure on the operating mechanism. Reshетенko et al. [9] confirmed the operating mechanism of a spatial fuel cell by studying segmented cells. They discovered that an increase in the backpressure not only improves the overall cell performance but also lowers activation and mass transport losses to improve the performance homogeneity. Zhang et al. [10] reported that, as the backpressure increases, the exchange current density of the reactants increases, and the gas diffusion from the catalyst layer to the active sites of the catalyst increases. Larbi et al. [11] studied the effect of pressure when the pressure at the anode and cathode were not equal, and found that the potential of the electrolyte depends on the cathode pressure. Rohendi et al. [12] confirmed that when the performance of the membrane electrode assembly (MEA) was degraded after an operating time of 100 h followed by the application of backpressure, the cell conductivity was improved, and the open circuit voltage (OCV) was maintained compared with that under ambient conditions. Lu et al. [13] applied a 3D computational

fluid dynamics (CFD) model to inspect the effect of pressure on the PEMFC performance and found that high backpressure leads to high relative humidity in the cathode channel, which contributes to high membrane water content.

In this PEMFC operation, the cathode processes account for most of the electrochemical losses in all the cells and have a crucial influence on the cell performance [14,15]. Therefore, many scientific studies have been conducted on the design and optimization of cathode channels to increase the performance and efficiency of fuel cells. Baik et al. [16] developed metallic bipolar plates with a multi-hole structure in the rib region to improve the cell performance at high current density. Application thereof to the cathode increased the current density by 37.8%. Kumar et al. [17] evaluated the performance of air-breathing PEMFCs by comparing the cathode channel design. Thomas et al. [18] researched the effect of changing the dimensions such as the width and depth of the cathode channel in open-cathode high-temperature PEMFCs. Henriques et al. [19] investigated the effect of the cathode geometry with the aim of improving the efficiency of portable PEMFCs and used a 3D CFD model to analyze the cell performance. However, an investigation of the fuel cell operation also requires the effect of the anode channel to be considered, as in Zhong's study [20]. Zhong et al. [20] optimized the anode parallel flow field structure to ameliorate starvation during PEMFC operation. Therefore, to maximize the performance of the fuel cell, it is necessary to examine the complex effect of both the cathode and anode channels. An understanding of this effect would require both of these channels to be optimized.

In a previous study [21], we analyzed the variation in the performance of fuel cells by changing the operating pressure and channel width of the serpentine bipolar plate. As the channel width was decreased and the operating pressure was increased, the maximum power density, which is a performance index of fuel cells, was enhanced. Moreover, the results confirmed that when bipolar plates with wide channels were used, the rate at which the performance increased as a result of the operating pressure was the most remarkable. To investigate the diffusion characteristics in the flow channel resulting from the change in these conditions, the Sherwood number (Sh), which is a dimensionless number representing the degree of diffusion acting perpendicular to the electrode, was introduced and discussed. Sh was derived as a correlation between the Reynolds (Re) and Schmidt (Sc) numbers. In this study, we examined the effect of these experimental settings on the performance of fuel cells under pressurized operating conditions while varying the channel width of the bipolar plates used in the anode and cathode. In this regard, it is considered that this research will fill the knowledge gap in this area. In particular, the effect on diffusion in the flow channel was analyzed by using anode and cathode bipolar plates that were mismatched. The diffusion characteristics in the channels of the fuel cells were investigated by analyzing the single-phase model using Sh followed by experimental verification of these results.

This study hypothesized that the mismatched channel would affect performance to some extent. In order to arrive at this hypothesis, an experiment was conducted with the mismatched situation, and a pressurized condition was also applied following the previous study [21]. Quantitative performance was secured for the experiment conducted in this way, and analysis was attempted by introducing a dimensionless number. This offers the possibility of discussing most flow scenarios using the diffusion characteristics, as in this study. At this time, by re-introducing dimensionless numbers based on previous experience, we investigate the way in which changes in the width of the anode and cathode flow channels along with the operating pressure improve the mass transport by analyzing the diffusion characteristics. The findings of this hydrodynamic-based study are expected to facilitate the design and optimization of the operation of fuel cells. The significance of this study lies therein that we conducted an experimental analysis of the diffusion that occurs in the flow channel.

2. Experimental

2.1. Configuration of Experiment

Figure 1 shows the experimental apparatus we constructed and the different anode and cathode plates we used. This setup enabled us to observe the change in the performance of the fuel cells when the flow channel widths of the anode and cathode bipolar plates were different, and the operating pressure was altered in that state. Figure 1a,b shows the bipolar plates with the same channel width of 1.0 mm for both the anode and cathode (A1C1), and with a different channel width of 1.0 mm for the anode and 0.3 mm for the cathode (A1C3), respectively. Figure 1c,d shows the bipolar plates with a different channel width of 0.3 mm for the anode and 1.0 mm for the cathode (A3C1), and with the same channel width of 0.3 mm for the anode and cathode (A3C3), respectively.

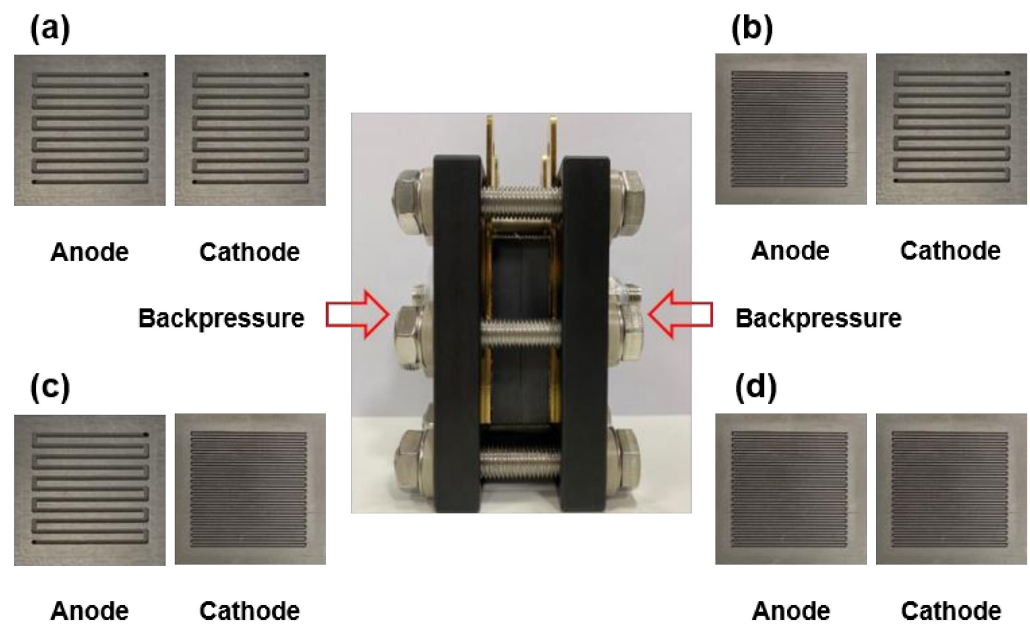


Figure 1. Schematic of the experiment: (a) Anodic channel width is 1.0 mm and cathodic channel width is 1.0 mm (A1C1), (b) anodic channel width is 0.3 mm and cathodic channel width is 1.0 mm (A3C1), (c) anodic channel width is 1.0 mm and cathodic channel width is 0.3 mm (A1C3), and (d) anodic channel width is 0.3 mm and cathodic channel width is 0.3 mm (A3C3).

The catalyst-coated membranes used in the experiments were identical for each experiment. The catalyst was prepared by mixing Pt/C (40 wt.% Pt, Johnson Matthey Inc., London, UK), Nafion[®] ionomer solution (5 wt.%, Sigma–Aldrich Inc., St. Louis, MO, USA), and isopropyl alcohol (Daejung Chemicals and Metals Co., Siheung, Korea). This solution was placed in a vial, agitated in a vortex mixer for 2 min, and placed in an ultrasonic cleaner for 60 min to ensure that the Pt/C was well dispersed. After that, a 25.4- μm -thick Nafion[®] 211 membrane (Dupont Inc., Wilmington, DE, USA) was placed on a hot plate heated to 80 °C, and the well-mixed catalyst solution was sprayed on the membrane evenly such that the reaction area on each side of the membrane was $2.24 \times 2.24 \text{ cm}^2$ (total area of 5 cm^2). The Pt loading on each side of the membrane was 0.12 mg/cm^2 . Together with the prepared catalyst coated membrane (CCM), 36BB gas-diffusion layers (SGL Carbon Inc., Wiesbaden, Germany), polytetrafluoroethylene-coated cloth gaskets ($t = 250 \mu\text{m}$), bipolar plates, current collectors, and end plates were assembled. A clamping torque of 60 kgf·m is applied to bolts when assembling the cell. This assembled single cell was connected to a test station (CNL Energy, Seoul, Korea). The fuel cells were operated at 70 °C, and fully humidified hydrogen, oxygen, and air were injected into the fuel cells at flow rates of 150, 200, and 800 cm^3/min . Backpressure was applied to the outlet vents of the anode and cathode to control the pressure inside the fuel cells.

2.2. Measurement

For each experiment, after sufficiently activating the cell using oxygen in the cathode, a pressurization experiment was conducted using air. Here, the process of activating the cell means when the power density converges to its maximum by continuously injecting oxygen. When the fuel cells were operated under pressurized conditions, the effect of imparting backpressure is referred to as the operating pressure in this study. Because the effect of applying backpressure to the anodic side does not affect the performance of the fuel cells significantly, the backpressure applied to the cathode was considered to be the operating pressure in this experiment. The backpressure levels we used were 0, 0.5, 1.0, and 3.0 bar. On the other hand, if the anode backpressure is not changed, the higher the cathode backpressure becomes, the greater is the pressure difference between the two sides, which can damage the membrane electrode assembly [22]. Therefore, the anode backpressure was appropriately changed to 0, 0.3, 0.6, and 2.1 bar according to the cathode backpressure. In each experiment, the current density–voltage (*j*-*V*) polarization curve and power density curve with maximum power density value were obtained, and used to analyze the performance. Electrochemical impedance spectroscopy (EIS) was performed using an electrochemical workstation (ZIVE SP2, WonA Tech Co., Seoul, Korea). The spectra were recorded after acquiring the *j*-*V* and power density curves. At this time, the electrochemical impedance spectrum was recorded at 0.85 V vs. a reversible hydrogen electrode (RHE). In addition, the diffusion characteristics in the channel were investigated to analyze the mass transport of the fuel cells. This was accomplished by calculating the non-dimensional numbers *Re*, *Sc*, and *Sh* using the experimental data obtained from the *j*-*V* curve, and the diffusion occurring on the side of the cathode was considered.

3. Results and Discussion

Figure 2 shows the polarization curves for (a) A1C1, (b) A3C1, (c) A1C3, and (d) A3C3. Figure 3 shows the same polarization curves for the different pressure levels of (a) 0, (b) 0.5, (c) 1.0, and (d) 3.0 bar. The cathode pressure drop is 0.045 bar for A1C1 and A3C1, and 3.004 bar for A1C3 and A3C3. This is obtained using the same method for calculating the cathode pressure drop in the previous study [21]. At this time, the cathode inlet pressure can be obtained by adding the atmospheric pressure and the backpressure applied to the outlet to the cathode pressure drop. For all combinations, as the operating pressure increased, the *j*-*V* curves tended to move upward and to the right, and the OCV also increased. As the operating pressure increases, the concentration of the reactant and the reaction rate increase, and as a result, the activation loss and concentration loss gradually decrease, and this is considered to be the reason for the curves shifting to the upper right [1]. The downward bending of the right end of the *j*-*V* curves intensified as the operating pressure increased. In addition, the partial pressure of the reaction gases increased, which increased the reversible voltage, which improved the OCV [10,23]. The *j*-*V* curve reflects the higher overall limiting current density resulting from the narrower channel width of the bipolar plate on the cathodic side of 0.3 mm (A1C3, A3C3) compared with the wider channel of 1.0 mm (A1C1, A3C1). In this experiment, the value of the actual limiting current density could not be obtained by measuring the voltage up to 0.35 V. Instead, the current density was calculated at 0 V by using auto fitting of the *j*-*V* curve. The current density at this time was assumed to be the limiting current density, which is expressed by the following equation:

$$j_L = nFD^{eff}\frac{c_R^0}{\delta} \quad (1)$$

where *n* is the number of electrons transferred in the reaction, *F* is Faraday's constant, *D^{eff}* is the effective reactant diffusivity, *c_R⁰* is the reactant bulk concentration value, and *δ* is the diffusion layer thickness. The effective reactant diffusivities were calculated based on the cathode and are provided in Table 1. Only the limiting current density of oxygen is considered when determining the mass transport losses of most fuel cells. This is because

oxygen diffuses more slowly than hydrogen, thus the limitation of mass transport by the movement of oxygen is generally much more severe than that of hydrogen [1,11]. The typical value for the effective reactant diffusivity, $0.01 \text{ cm}^2/\text{s}$ [1], is similar to the corresponding value calculated in this work, which is therefore considered to be appropriately calculated. Because the effective reactant diffusivity values of A1C3 and A3C3 are larger than those of A1C1 and A3C1, the value of the limiting current density seems to mirror this trend.

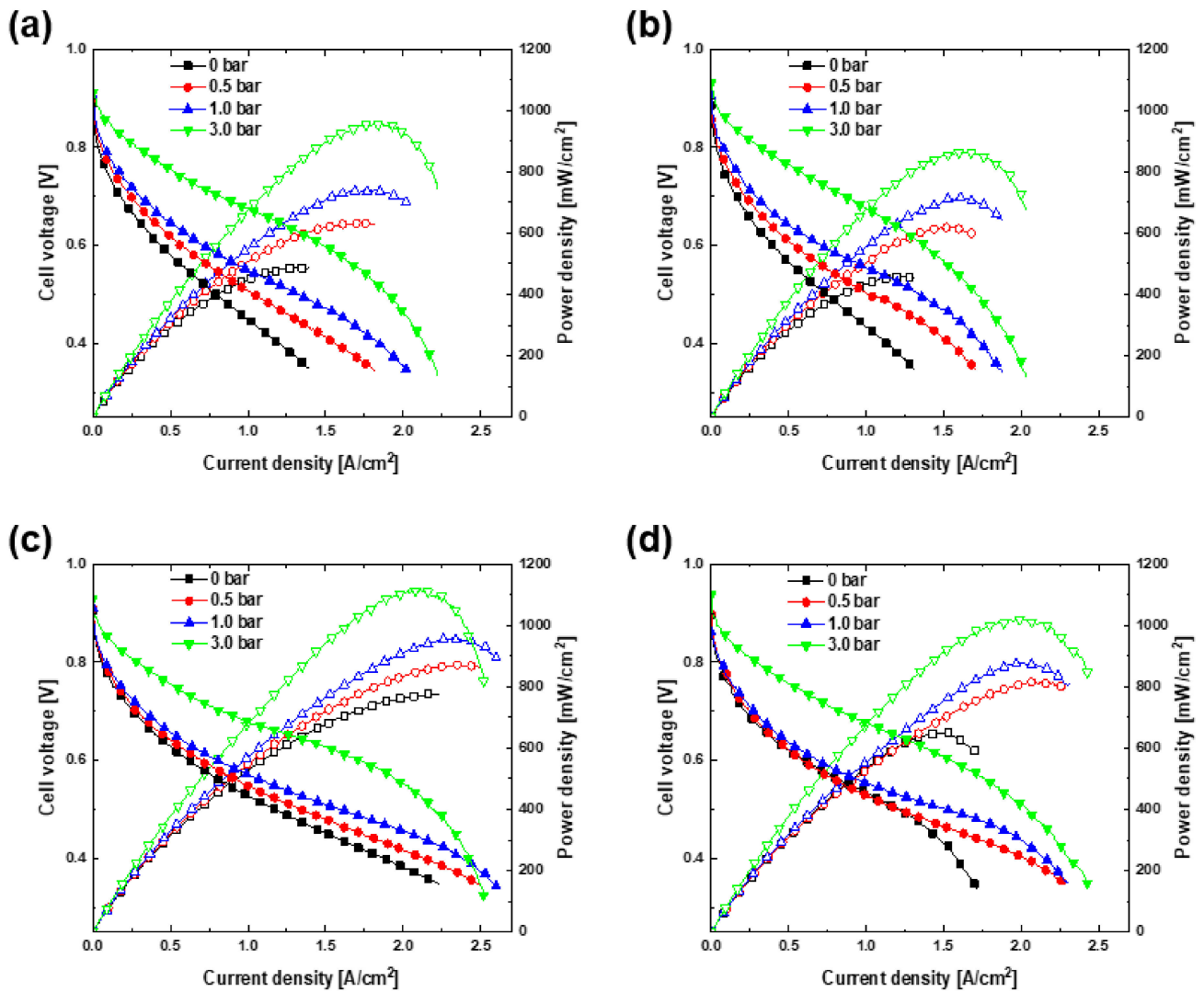


Figure 2. Performance comparison of (a) A1C1, (b) A3C1, (c) A1C3, and (d) A3C3.

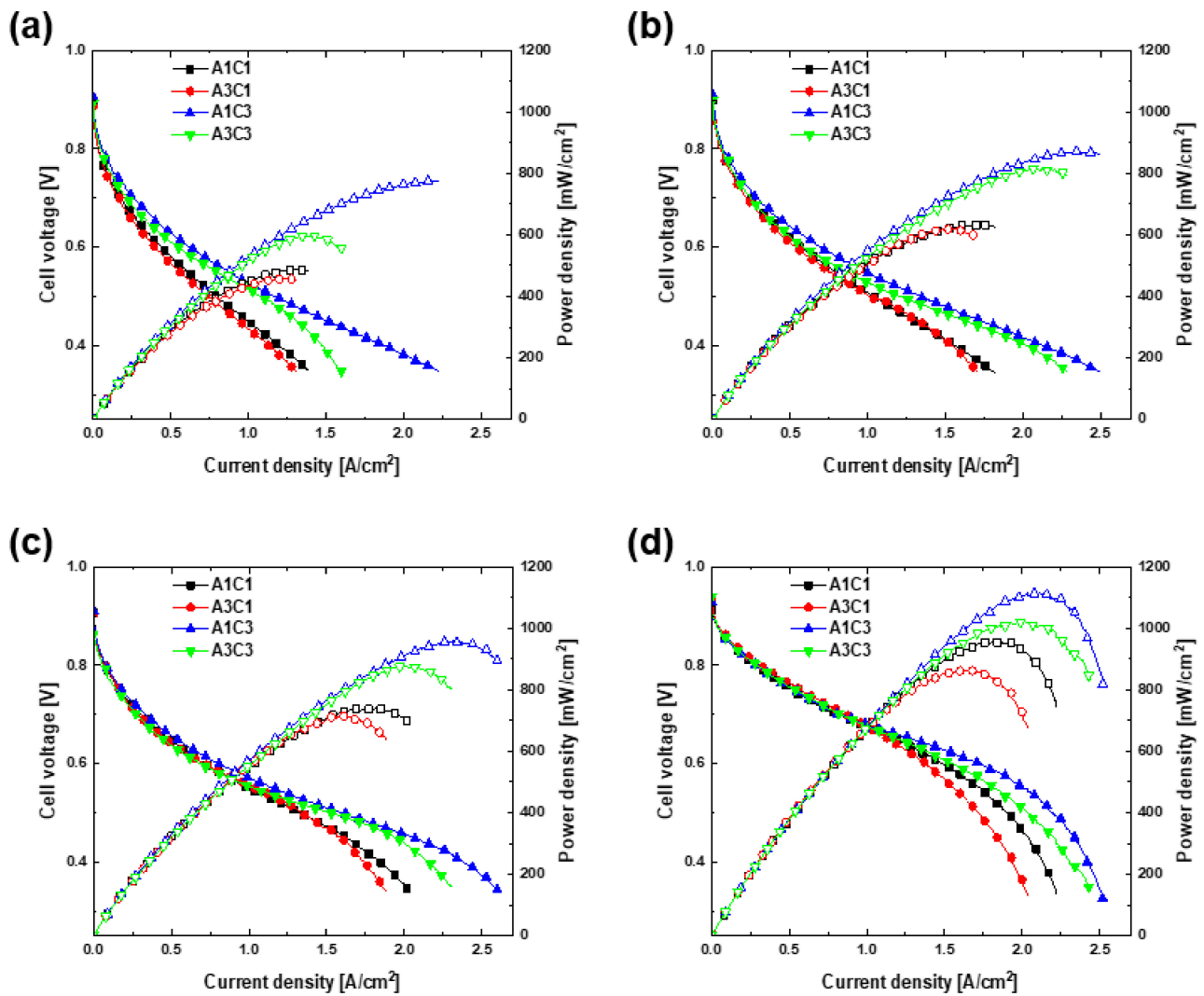


Figure 3. Performance comparison in (a) 0, (b) 0.5, (c) 1.0, and (d) 3.0 bar.

Table 1. Effective reactant diffusivities and non-dimensional parameters (Re , Sc , and Sh).

P [bar]	$D^{eff} [10^{-6} \text{ m}^2/\text{s}]$				Re			
	A1C1	A3C1	A1C3	A3C3	A1C1	A3C1	A1C3	A3C3
0	2.168	2.063	3.530	2.391	775	775	1463	1463
0.5	1.660	1.522	2.284	2.029	1162	1162	2194	2194
1.0	1.265	1.154	1.601	1.412	1548	1548	2925	2925
3.0	0.607	0.547	0.673	0.679	3093	3093	5842	5842
P [bar]	Sc				Sh			
	A1C1	A3C1	A1C3	A3C3	A1C1	A3C1	A1C3	A3C3
0	13.625	14.320	8.369	12.355	0.0737	0.0700	0.0667	0.0427
0.5	10.342	11.280	7.515	8.459	0.0840	0.0769	0.0608	0.0534
1.0	9.563	10.480	7.557	8.565	0.0849	0.0773	0.0550	0.0481
3.0	9.146	10.153	8.249	8.180	0.0806	0.0725	0.0443	0.0447

The power density curves in Figures 2 and 3 confirmed that the peak power density increased as the operating pressure increased. In the case of A1C1, the maximum power density was $488 \text{ mW}/\text{cm}^2$ under ambient conditions and increased to $959 \text{ mW}/\text{cm}^2$ when the cell was pressurized to 3.0 bar. In the case of A3C1, the maximum power density was

461 and 868 mW/cm^2 at 0 and 3.0 bar, respectively. These values increased to 776 mW/cm^2 at 0 bar and 1115 mW/cm^2 at 3.0 bar in the case of A1C3, the highest of all the operating pressures among the four experimental sets. Lastly, in the case of A3C3, the corresponding values were 650 and 1024 mW/cm^2 at 0 and 3.0 bar, respectively. According to the experimental results, the performance of the fuel cells is largely determined by the width of the flow channel on the cathodic side. In Figure 3, it is remarkable that the polarization curves are divided according to the width of the cathodic flow channel. Compared with A1C1 and A3C1, the j - V curves of A1C3 and A3C3, which have narrow cathodic flow channels, are extended to the upper right, and accordingly, the power density curves are also different. When the operating pressure reached 3.0 bar, the slope of the high current density portion of all sets of j - V curves increased. This is responsible for the active reaction of high-concentration reactants as a result of the high pressure, causing flooding [24]. In addition, for the two cases in which the width of the flow channel on the cathodic side is the same, the performance differs slightly as the width of the flow channel on the anodic side is different. A comparison of the performance by comparing the power density reveals that A1C3 outperforms A3C3, and the performance of A1C1 is superior to that of A3C1. In the case of A1C3 and A3C3, the overall performance was excellent owing to the narrow width of the cathode channel, although A1C3 delivered excellent performance in the low-voltage region with high maximum power density. This is attributed to a change in the distribution patterns of the channel and rib. Liu et al. [25] showed that the rib-to-channel (RTC) distribution outperforms the rib-to-rib (RTR) distribution. Here, the RTR and RTC distributions refer to structures in which the ribs of one bipolar plate face the ribs of the other bipolar plate, and the ribs of one bipolar plate face the flow channel of the other bipolar plate, respectively. They confirmed that the performance in both cases was the same in the high-voltage region of the cell, but the performance of the RTC distribution was higher in the low-voltage region. Hoppe et al. [26] observed that CCM was bent through a computer tomograph in the state of the flow field plate misalignment similar to the concept of RTC distribution above but confirmed that there was no significant difference in performance compared to the case without misalignment. However, when the pressurization experiment is performed on flow field plate misalignment, it is considered that the CCM will be damaged beyond bending, and the contact resistance will increase, which will significantly affect the performance [27,28]. The advantage of the experimental setting used in this study is that because the widths of the flow channels of both bipolar plates differ, one channel and several ribs on the other side overlap. This maximizes the performance of the electrochemical reaction by supporting the MEA and reducing the contact resistance, even if the cell were to be operated under pressure. In fact, there was no severe noticeable damage when checking the MEA after the pressurization test up to 3.0 bar. On the other hand, A1C1 and A3C1 exhibited the opposite tendency. A1C1, for which both bipolar plates have the same flow channel width, seems to have more effective mass transport in the low-voltage region. Hydrogen, the reactant on the anodic side, has outstanding diffusivity; thus, the wider the flow channel, the higher the performance because a large amount of hydrogen exists in the channel [1,29]. An anode with a narrow flow channel would generate differential pressure; so, diffusion to the GDL is considered to be difficult. Therefore, the performance of the fuel cells is excellent under the same conditions when the flow channel on the cathodic side is narrow and the flow channel on the anodic side is wide. In previous research, because the same bipolar plate was used for the anode and cathode, the performance improved as the flow channel was unconditionally narrow. However, in this study, the influence of the anodic flow channel was confirmed by changing the width of the flow channel of both of the bipolar plates.

To investigate the diffusion that occurs in the cathode flow channel when the two bipolar plates are mismatched in terms of their channel width, the dimensionless numbers Re , Sc , and Sh were calculated as in previous research [21]. These values are summarized in Table 1. In this case, they are estimated in single-phase fluid. First, the calculated values of Re depend on the width of the cathode channel. The overall Re values were higher when the

cathode flow channel was narrower, and Re developed as the operating pressure increased. A larger Re indicates the momentum in the channel; that is, the flow is active, which means that the diffusion from the channel to the catalyst layer improves. On the other hand, Sc is generally small when the cathode flow channel is narrow and tends to decrease as the operating pressure increases. This trend in Sc indicates that the hydrodynamic boundary layer becomes shorter, and mass transport predominates. This implies that the narrower the cathode flow channel and the higher the operating pressure are, the more active the diffusion in the channel becomes. Unlike the value of Re , the value of Sc changes as the width of the anode channel changes when the width of the cathode channel remains the same. Although the calculation of this non-dimensional number is done on the cathode side, the value of Sc , which means the overall diffusion, changes in this situation. This shows that the width of the anode channel also affects the diffusion in the cathode channel, and that diffusion is excellent when the anode channel is wide. The values of Sh , which is a non-dimensional number representing vertical diffusion, are small when the cathode channel is narrow and follows a decreasing trend as the operating pressure increases. By changing the width of the anodic flow channel, which was not investigated in previous research, the value of Sh was found to be large for a wide anodic channel and the same cathodic channel width. Vertical diffusion decreases because of excessive flooding in the flow channel as the overall diffusion increases when the cathodic channel is narrow and the operating pressure increases; however, it seems that this phenomenon is more effectively eliminated by increasing the anodic channel width. Therefore, to summarize the analysis based on the calculation of these dimensionless numbers, the overall diffusion improves when the cathodic flow channel, which greatly affects the performance, is narrow, and the operating pressure increases. The width of the anodic channel also affects the diffusion on the cathodic side. The results also showed a wide anodic channel not only improves the vertical diffusion but also the overall diffusion, which has a positive effect on mass transport. In the same way as in the previous research [21], a correlation of mismatched cases is derived from the calculated non-dimensional numbers in Table 1. This is as follows:

$$Sh = 0.784Re^{-0.265}Sc^{-0.215} \quad (2)$$

It is slightly different from the correlation obtained in previous research, but it seems to be because there is a change in the flow channel width on the anode compared to the general study. Since the bipolar plates of the anode and cathode are different, as described above, the overlapping of one channel and several ribs or the overlapping of one rib and several channels is considered to create uncertain variables.

Figure 4 shows the change rate of the maximum power density and enables us to observe the variation in the performance of fuel cells for each experimental set by using the power density curve. The rate of change is the amount of variation in the maximum power density at each operating pressure compared to the maximum power density at 0 bar. In the case of A1C1, when the backpressure was increased to 3.0 bar, the change rate was 96.5%, showing the largest shift. At the same operating pressure, the change rate for A3C1 was 88.3%, showing a relatively large increase in performance. The corresponding change rates of A1C3 and A3C3 were 43.7% and 57.5%, respectively. As the operating pressure increased, the performance variation of A1C1 and A3C1, which had wide cathodic channels, exhibited a remarkable increase in performance, but the use of an alternative width for the anodic channel did not seem to have a significant effect on the magnitude of the performance change. Hence, for absolute performance, it is more effective to use a bipolar plate with a narrow channel on the cathode; however, when the fuel cells are operated under pressure, using a wider channel on the cathode increases the performance to a greater extent because its change rate compared to the initial performance is larger.

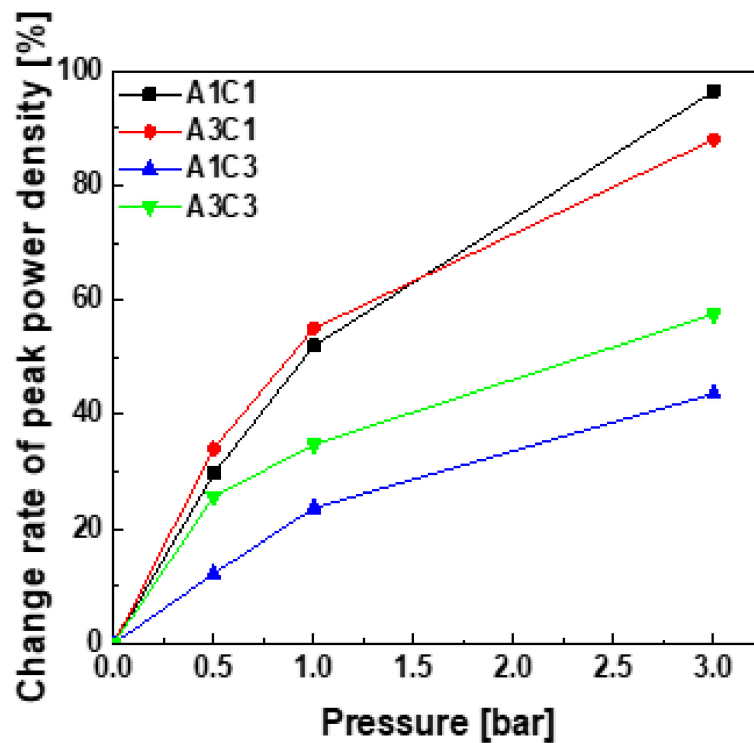


Figure 4. Change rate of peak power density by backpressure.

To further analyze the polarization curves above, the EIS results of each experiment were evaluated, as summarized in Figure 5. At this time, because the oxidation reaction of hydrogen is very fast, the impedance spectrum of the full cell was almost the same as the impedance spectrum of the cathode. In addition, because the electrochemical impedance spectrum was recorded at a low current density, the concentration loss was not detected when the spectra were recorded. Accordingly, the reaction that occurred in the cells in this experiment was modeled as an equivalent circuit. The equivalent circuit consists of the ohmic resistance (R_{Ω}), charge transfer resistance (R_{ct}), and constant phase element (CPE), representing the double-layer capacitance and appears in the top left corner of each subfigure in Figure 5. These spectra present the impedance when the voltage is 0.85 V vs. RHE. The size of each semicircle represents the activation loss, and the first value of Z_{real} when $-Z_{im}$ is zero indicates the ohmic loss [1,30]. In all cases, the graphs directly indicate that the activation loss decreases as the backpressure increases. The activation loss of A1C1 decreases from $5.61 \Omega \cdot \text{cm}^2$ to 4.13 , 2.25 , and $0.98 \Omega \cdot \text{cm}^2$ with increasing operating pressure and that of A3C1 decreases from $6.37 \Omega \cdot \text{cm}^2$ to 3.55 , 2.47 , and $1.04 \Omega \cdot \text{cm}^2$. Likewise, that of A1C3 decreases from $3.62 \Omega \cdot \text{cm}^2$ to 2.73 , 2.21 , and $1.01 \Omega \cdot \text{cm}^2$, and that of A3C3 decreases from $4.46 \Omega \cdot \text{cm}^2$ to 3.65 , 3.11 , and $1.01 \Omega \cdot \text{cm}^2$. The magnitude of the activation loss of A1C3 and A3C3 when no operating pressure was applied was smaller than that of the other two combinations (A1C1 and A3C1). In all cases, as the operating pressure increased, the magnitude of the activation loss decreased, and when the operating pressure was 3.0 bar, the magnitude of the activation loss became almost the same. Moreover, the ohmic loss was shown in the inset on the right side of each subfigure in Figure 5. In most cases, as the operating pressure increased, the tendency of the value of the ohmic loss to decrease was confirmed. In addition, the ohmic loss did not differ distinctly between the general situation and the state in which the bipolar plates were mismatched. Even when both bipolar plates were mismatched and the cells were pressurized, the loss due to contact resistance seemed negligible.

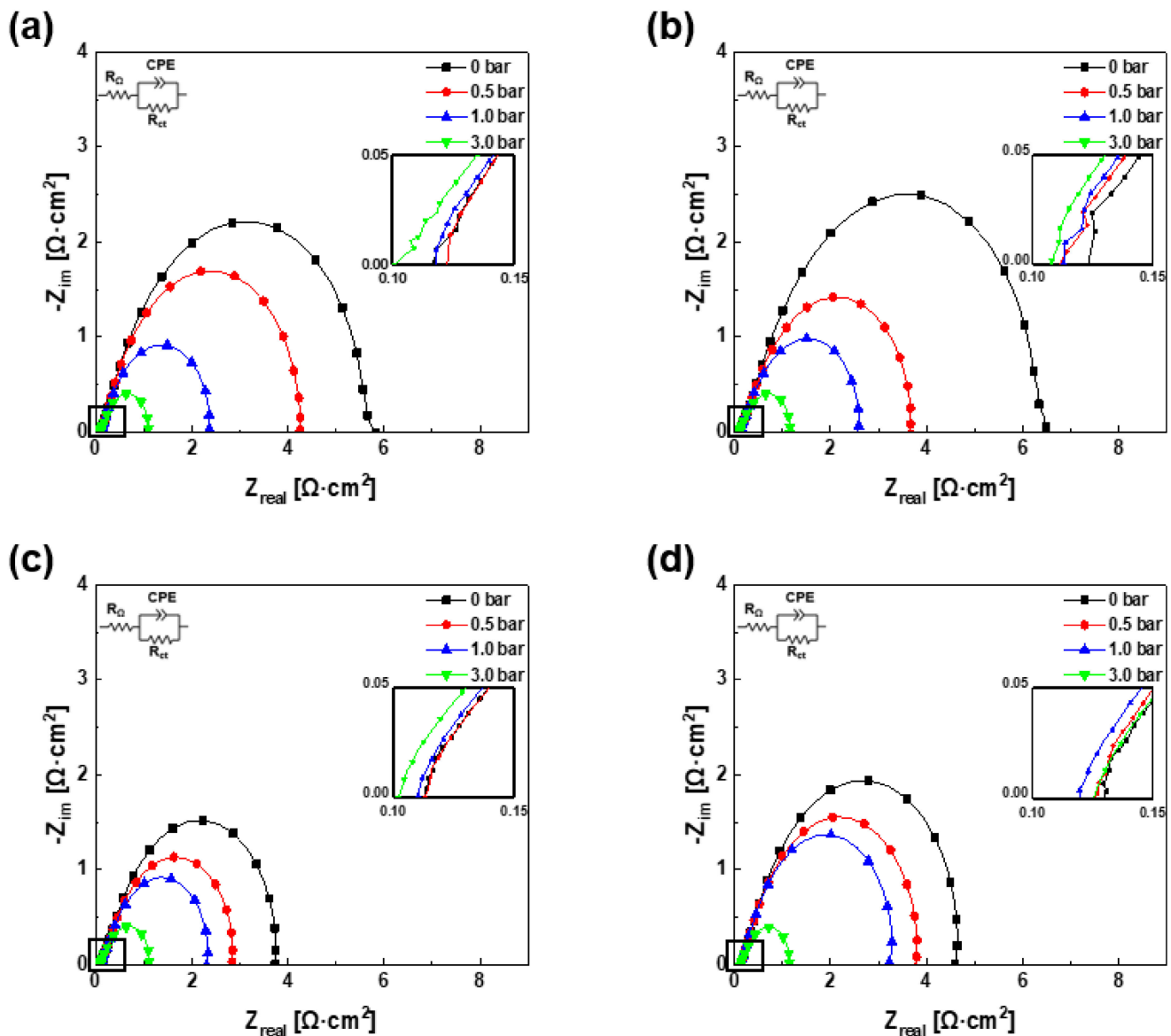


Figure 5. EIS measurements at 0.85 V (vs. RHE) of the PEMFCs with (a) A1C1, (b) A3C1, (c) A1C3, and (d) A3C3.

4. Conclusions

When the width of the flow channels of the cathode and anode are mismatched the effect of diffusion changes, resulting in a difference in performance. Apart from this, the operating pressure and channel width have a combined impact on the performance of the fuel cells. These operating conditions and the channel width can be adjusted to optimize the overall performance. The experimental set was configured using four combinations (A1C1, A1C3, A3C1, A3C3) of two different bipolar plates with channel widths of 1.0 and 0.3 mm. This set was used to conduct a pressurization experiment to analyze the change in the performance of each, and this was discussed using the j-V curve and EIS data. With the narrow cathode channel, the performance increased as the backpressure increased. In particular, the maximum power density, which is one of the performance indicators of fuel cells, of the four combinations was compared. The maximum power densities of A1C3 and A3C3, which have a narrow cathode channel, are 960 mW/cm² and 876 mW/cm² at 1.0 bar, respectively. In the case of A1C1 and A3C1, both of which have a wide cathode channel, the corresponding densities are 742 and 715 mW/cm² at 1.0 bar, respectively. The variation in the width of the anodic flow channel was found to affect the performance. Under the

same experimental conditions, the performance is expected to be excellent when a narrow cathodic channel is combined with a wide anodic channel. The results confirmed that there is no additional loss of contact resistance even if both bipolar plates are mismatched and the operation is pressurized. In addition, by calculating the non-dimensional numbers Re , Sc , and Sh , the width of the anodic flow channel is determined to influence the diffusion in the cathodic flow channel. When the cathodic flow channel is narrow, the value of Re increases and the value of Sc decreases. The value of Sh decreases when the cathodic flow channel is narrow and the operating pressure increases, and Sh increases when the anodic flow channel is wide. This means that the anodic bipolar plate with a wide channel improves not only the vertical diffusion but also the overall diffusion, thereby promoting mass transport. This study will provide vision into the property of the fuel cell diffusion effect, and is expected to lead to the following future work: diffusion analysis by comparison of impedance spectrum at various voltage ranges, checking stability by long-term testing under severe conditions such as 3.0 bar operating pressure, and analyzing the surface at that time, etc. The detail surface analysis of the pre- and post-performance of electrodes in a harsh environment with high operating pressure and the mismatched situation of channels is a future scope of our future work.

Author Contributions: Conceptualization, H.K. and T.P.; methodology, H.K. and T.P.; software, H.K.; validation, H.K., G.K., J.K. and D.K.; formal analysis, H.K.; investigation, H.K., G.K., J.K., D.K., O.K., H.Y., H.C. (Hyeonjin Cha) and H.C. (Heesoo Choi); resources, H.K. and G.K.; data curation, H.K.; writing—original draft preparation, H.K.; writing—review and editing, H.K.; visualization, H.K.; supervision, H.K. and T.P.; project administration, H.K. and T.P.; funding acquisition, T.P. All authors have read and agreed to the published version of the manuscript.

Funding: This work was financially supported by an NRF grant funded by the Ministry of Science and ICT (Grant No. 2020R1C1C1009191).

Institutional Review Board Statement: Not applicable.

Informed Consent Statement: Not applicable.

Data Availability Statement: Not applicable.

Conflicts of Interest: The authors declare no conflict of interest.

References

1. O'hayre, R.; Cha, S.W.; Colella, W.; Prinz, F.B. *Fuel Cell Fundamentals*; Wiley: Hoboken, NJ, USA, 2009; ISBN 9780387735313.
2. Gasteiger, H.A.; Markovic, N.M. Just a Dream—Or Future Reality? *Science* **2009**, *324*, 48–49. [[CrossRef](#)] [[PubMed](#)]
3. Aiyejina, A.; Sastry, M.K.S. PEMFC Flow Channel Geometry Optimization: A Review. *J. Fuel Cell Sci. Technol.* **2011**, *9*, 011011. [[CrossRef](#)]
4. Kim, K.; Kim, T.; Lee, K.; Kwon, S. Fuel cell system with sodium borohydride as hydrogen source for unmanned aerial vehicles. *J. Power Sources* **2011**, *196*, 9069–9075. [[CrossRef](#)]
5. Cheema, T.A.; Kim, G.M.; Lee, C.Y.; Kwak, M.K.; Kim, H.-B.; Park, C.W. Effects of composite porous gas-diffusion layers on performance of proton exchange membrane fuel cell. *Int. J. Precis. Eng. Manuf. Technol.* **2014**, *1*, 305–312. [[CrossRef](#)]
6. Wang, X.-D.; Duan, Y.; Yan, W.-M. Novel serpentine-baffle flow field design for proton exchange membrane fuel cells. *J. Power Sources* **2007**, *173*, 210–221. [[CrossRef](#)]
7. Wang, X.-D.; Duan, Y.-Y.; Yan, W.-M.; Peng, X.-F. Effects of flow channel geometry on cell performance for PEM fuel cells with parallel and interdigitated flow fields. *Electrochim. Acta* **2008**, *53*, 5334–5343. [[CrossRef](#)]
8. Chen, Y.-S.; Peng, H. Predicting current density distribution of proton exchange membrane fuel cells with different flow field designs. *J. Power Sources* **2011**, *196*, 1992–2004. [[CrossRef](#)]
9. Reshetenko, T.V.; Bender, G.; Bethune, K.; Rocheleau, R. Systematic study of back pressure and anode stoichiometry effects on spatial PEMFC performance distribution. *Electrochim. Acta* **2011**, *56*, 8700–8710. [[CrossRef](#)]
10. Zhang, J.; Song, C.; Zhang, J.; Baker, R.; Zhang, L. Understanding the effects of backpressure on PEM fuel cell reactions and performance. *J. Electroanal. Chem.* **2013**, *688*, 130–136. [[CrossRef](#)]
11. Larbi, B.; Alimi, W.; Chouikh, R.; Guizani, A. Effect of porosity and pressure on the PEM fuel cell performance. *Int. J. Hydrogen Energy* **2013**, *38*, 8542–8549. [[CrossRef](#)]
12. Rohendi, D.; Majlan, E.; Mohamad, A.; Daud, W.; Kadhum, A.; Shyuan, L. Effects of temperature and backpressure on the performance degradation of MEA in PEMFC. *Int. J. Hydrogen Energy* **2015**, *40*, 10960–10968. [[CrossRef](#)]

13. Lu, J.B.; Wei, G.H.; Zhu, F.J.; Yan, X.H.; Zhang, J.L. Pressure Effect on the PEMFC Performance. *Fuel Cells* **2019**, *19*, 211–220. [[CrossRef](#)]
14. Sun, W.; Peppley, B.A.; Karan, K. Modeling the Influence of GDL and flow-field plate parameters on the reaction distribution in the PEMFC cathode catalyst layer. *J. Power Sources* **2005**, *144*, 42–53. [[CrossRef](#)]
15. Zhao, C.; Xing, S.; Chen, M.; Liu, W.; Wang, H. Optimal Design of Cathode Flow Channel for Air-Cooled PEMFC with Open Cathode. *Int. J. Hydrogen Energy* **2020**, *45*, 17771–17781. [[CrossRef](#)]
16. Baik, K.D.; Seo, I.S. Metallic bipolar plate with a multi-hole structure in the rib regions for polymer electrolyte membrane fuel cells. *Appl. Energy* **2018**, *212*, 333–339. [[CrossRef](#)]
17. Kumar, P.M.; Kolar, A.K. Effect of cathode design on the performance of an air-breathing PEM fuel cell. *Int. J. Hydrogen Energy* **2010**, *35*, 671–681. [[CrossRef](#)]
18. Thomas, S.; Bates, A.; Park, S.; Sahu, A.; Lee, S.C.; Son, B.R.; Kim, J.G.; Lee, D.-H. An experimental and simulation study of novel channel designs for open-cathode high-temperature polymer electrolyte membrane fuel cells. *Appl. Energy* **2016**, *165*, 765–776. [[CrossRef](#)]
19. Henriques, T.; César, B.; Branco, P.C. Increasing the efficiency of a portable PEM fuel cell by altering the cathode channel geometry: A numerical and experimental study. *Appl. Energy* **2010**, *87*, 1400–1409. [[CrossRef](#)]
20. Zhong, D.; Lin, R.; Liu, D.; Cai, X. Structure optimization of anode parallel flow field for local starvation of proton exchange membrane fuel cell. *J. Power Sources* **2018**, *403*, 1–10. [[CrossRef](#)]
21. Kim, H.; Kim, J.; Kim, D.; Kim, G.H.; Kwon, O.; Cha, H.; Choi, H.; Yoo, H.; Park, T. Mass diffusion characteristics on performance of polymer electrolyte membrane fuel cells with serpentine channels of different width. *Int. J. Heat Mass Transf.* **2021**, *183*, 122106. [[CrossRef](#)]
22. Ge, S.-H.; Yi, B.-L. A mathematical model for PEMFC in different flow modes. *J. Power Sources* **2003**, *124*, 1–11. [[CrossRef](#)]
23. Wang, L.; Liu, H. Performance studies of PEM fuel cells with interdigitated flow fields. *J. Power Sources* **2004**, *134*, 185–196. [[CrossRef](#)]
24. Li, H.; Tang, Y.; Wang, Z.; Shi, Z.; Wu, S.; Song, D.; Zhang, J.; Fatih, K.; Zhang, J.; Wang, H.; et al. A review of water flooding issues in the proton exchange membrane fuel cell. *J. Power Sources* **2008**, *178*, 103–117. [[CrossRef](#)]
25. Liu, Z.; Zhang, H.; Wang, C.; Mao, Z. Numerical simulation for rib and channel position effect on PEMFC performances. *Int. J. Hydrogen Energy* **2010**, *35*, 2802–2806. [[CrossRef](#)]
26. Hoppe, E.; Janßen, H.; Müller, M.; Lehnert, W. The impact of flow field plate misalignment on the gas diffusion layer intrusion and performance of a high-temperature polymer electrolyte fuel cell. *J. Power Sources* **2021**, *501*, 230036. [[CrossRef](#)]
27. Lee, W.-K.; Ho, C.-H.; Van Zee, J.; Murthy, M. The effects of compression and gas diffusion layers on the performance of a PEM fuel cell. *J. Power Sources* **1999**, *84*, 45–51. [[CrossRef](#)]
28. Uzundurukan, A.; Bilgili, M.; Devrim, Y. Examination of compression effects on PEMFC performance by numerical and experimental analyses. *Int. J. Hydrogen Energy* **2020**, *45*, 35085–35096. [[CrossRef](#)]
29. Burlatsky, S.; Atrazhev, V.; Cipollini, N.; Condit, D.; Erikhman, N. Aspects of PEMFC Degradation. *ECS Trans.* **2006**, *1*, 239–246. [[CrossRef](#)]
30. Cooper, K.; Smith, M. Electrical test methods for on-line fuel cell ohmic resistance measurement. *J. Power Sources* **2006**, *160*, 1088–1095. [[CrossRef](#)]